



# CHORUS

This is the accepted manuscript made available via CHORUS. The article has been published as:

## Current-Driven Dyakonov-Shur Instability in Ballistic Nanostructures with a Stub

G. R. Aizin, J. Mikalopas, and M. Shur

Phys. Rev. Applied **10**, 064018 — Published 7 December 2018

DOI: [10.1103/PhysRevApplied.10.064018](https://doi.org/10.1103/PhysRevApplied.10.064018)

## Current driven Dyakonov-Shur instability in ballistic nanostructures with a stub

G. R. Aizin<sup>1\*</sup>, J. Mikalopas<sup>1</sup>, and M. Shur<sup>2†</sup>

<sup>1</sup> Kingsborough College, The City University of New York, Brooklyn, N, 11235, USA

<sup>2</sup> Rensselaer Polytechnic Institute, Troy, NY 12180, USA

We developed a compact model for the THz plasmonic unstable structures with the tunable narrow channel regions of an increased width (called plasmonic “stubs”) using the transmission line analogy and derived the dispersion equations describing unstable plasmons. The solutions of the dispersion equations in the plasmonic systems with the electron drift derived using the hydrodynamic model and generalized to account for the stubs illustrate the device physics and could be used for design and characterization of the THz plasmonic electronic sources. Our results show that adding stubs allows one to control the Dyakonov-Shur instability in plasmonic field effect transistors by optimizing the boundary conditions, controlling the plasma velocity, and making it possible to drive periodic plasmonic structures wirelessly avoiding the contact problems.

\*gaizin@kbcc.cuny.edu  
†shurm@rpi.edu

## I. INTRODUCTION

The feature sizes of field effect transistors have reached the dimensions comparable or smaller than the mean free path of electrons for collisions with impurities and lattice vibrations. The minimum feature size of silicon CMOS is now 7 nm (compared with about 30 nm mean free path for silicon at room temperature). At such dimensions the effects of the electron inertia are pronounced and the ballistic or quasi-ballistic transport [1] becomes dominant. The electron inertia is responsible for the excitation and propagation of the waves of the electron density – the plasmonic modes - that affect the transistor operation. The excitation of the plasmonic modes by an impinging terahertz radiation and their rectification in the resonant or non-resonant regimes have been used for the detection and mixing of the THz radiation [2] by silicon [3], InGaAs [4], GaN [5], and graphene [6] based field effect transistors. The instability of the plasmonic modes driven by a direct current in the ballistic regime (called the Dyakonov-Shur (DS) instability) enables the THz generation [7]. The plasmonic THz detectors performance is already comparable or superior to other THz detectors. However, the experimental observation of the DS instability [8] has been difficult. Another proposed approach to the THz generation was to use a so-called “plasmonic boom” with the generation occurring due to the electron velocity repeatedly exceeding and dropping below the plasma wave velocity [9,10]. So far, the plasmonic boom generation has not been demonstrated. Developing efficient, high power, and compact THz electronic sources remains the key goal of the THz electronic technology.

Several technological and physics-based problems must be solved to achieve this goal. First is the problem of the boundary conditions. The boundary conditions optimal for the DS instability are the short circuit between the source and the gate and open circuit between the drain and the gate [7]. This is difficult to implement at THz frequencies. The second problem is a small feature size (in the nanometer range) compared to the wavelength of the THz radiation (~300 micron at 1 THz). This makes it difficult to capture a large fraction of the impinging THz beam for the detection or match the device impedance for the emission. Grating gate device structures [11-13] could alleviate this second problem and were recently shown to be suitable for the implementation of the DS instability [14]. However, another problem is how to ensure the same gate-to-channel voltages in the field effect transistor channels connected in series [15].

Our recent paper [16] proposed addressing these problems by introducing the narrow regions protruding from the channel and having tunable electrical parameters, see Fig. 1a. We called these regions plasmonic stubs. We showed that the stubs could modify and optimize the boundary conditions and the input and output impedances. They can also slow down the plasma waves in a tunable way (making it easier to achieve the plasmonic boom) and could be used to match the plasmonic boundary conditions at the interfaces between different regions in the channel. In this paper, we analyze the effect of the stubs on the DS plasmonic instability and show that the stub design enables an efficient THz generation and could be applied for developing multi gated THz structures pumped by the RF radiation.

As shown in Ref. [16], the stub introduces impedance  $Z_{st}$  into the gated electron channel that can be viewed as a plasmonic waveguide. In this model, the solution of the hydrodynamic equations together with the Poisson equation in the 2D FET electron channel describes the plasma wave propagating along the FET plasmonic waveguide. Narrow regions protruding from the channel can be considered as the stubs attached to this plasmonic waveguide. If the width of

these regions is small in comparison with the plasmon wavelength in the 2D channel then the junction of the stub to the channel is a well-defined point. The impedance of the stub  $Z_{st}$  can be found by solving the same hydrodynamic and the Poisson equations for the plasma waves propagating along the stub 2D channel in the direction perpendicular to the 2D FET channel with the appropriate boundary conditions at the stub open end. Our approximation is solving two one-dimensional systems of equations: one for the channel and the other one for the stub. This approximation ignores the transition region between these two perpendicular one-dimensional solutions, which is justified if the electron-electron collision length is much smaller than all characteristic geometric parameters of the system, i.e. in the hydrodynamic model. Also, the widths of both the channel and the stub defining the geometric size of the transition region must be much smaller than the plasmon wavelength. Qualitatively, all the stubs with the width much smaller than the 2D channel length can be represented by impedances that could be tuned by the stub length and electron concentration from minus to plus infinity in complete analogy to the stubs used in the electrical transmission lines. A more accurate analysis of the effect of the transition region will require the 2D solution that should also account for the viscosity of the electronic fluid and for the surface scattering.

Impedance  $Z_{st}$  could vary from negative to positive infinity at the plasma frequency depending on the stub length  $l$ , width  $W_1$ , and 2D electron density in the stub. The stub effectively splits the plasmonic cavity between the source and the drain into two cavities: one between the source contact and the stub and the other one between the stub and the drain. These cavities have the terminating impedances  $Z_{gs}$  and  $Z_{st}$  and  $Z_{st}$  and  $Z_{gd}$ , respectively, as shown in the equivalent electric circuit in Fig. 1b. Here,  $Z_{gs}(Z_{gd})$  is the impedance between the gate and the source (drain) contact. The plasma frequency in each cavity depends on the cavity length and the electron drift velocity. As shown below, changing the stub length and its position in the channel and tuning the drift velocity one can change  $Z_{st}$  over a wide range thus creating boundary conditions suitable for the DS instability in the cavities regardless of the values  $Z_{gs}$  and  $Z_{gd}$ . Hence, the results presented in this paper show that adding stubs allows one to control the DS instability in plasmonic field effect transistors by optimizing the boundary conditions, controlling the plasma velocity, and making it possible to drive periodic plasmonic structures wirelessly avoiding the contact problems.

## II. BASIC EQUATIONS

Plasma waves propagating between the source and the drain contacts ( $x$ -axis) in the gated 2D electron layer ( $z = 0$ ) biased by a dc current can be described within the hydrodynamic model of the 2D electron fluid by the Euler equation and the continuity equation as

$$\begin{aligned} \frac{\partial v}{\partial t} + v \frac{\partial v}{\partial x} &= \frac{e}{m^*} \frac{\partial \varphi}{\partial x} \\ \frac{\partial n}{\partial t} + \frac{\partial(nv)}{\partial x} &= 0, \end{aligned} \tag{1}$$

where  $n(x, t)$  and  $v(x, t)$  are the local electron density and the velocity in the plasma wave, respectively,  $\varphi(x, z = 0, t)$  is electric potential in the 2D layer,  $-e$  is the electron charge and  $m^*$  is the effective electron mass. The hydrodynamic approach is justified if the time of the electron-electron collisions is the shortest electron characteristic time in the system. In the Euler equation,

we omitted the pressure gradient term since in the gated 2D channels this term is much smaller than the field term. We also neglected the effect of the electron collisions with phonons and impurities assuming the ballistic transport with respect to these collisions ( $\omega\tau \gg 1$ , where  $\omega$  is the plasmon frequency and  $\tau$  is the collision time).

Eqs. (1) for 2D electron fluid with a dc bias could be linearized with respect to the small fluctuations of electron density  $\delta n(x, t)$  and velocity  $\delta v(x, t)$  by assuming that  $n(x, t) = n_0 + \delta n$  and  $v(x, t) = v_0 + \delta v$  where  $n_0$  and  $v_0$  are the equilibrium electron density and constant electron drift velocity, respectively. We also assume that  $\delta n$  is linked to the fluctuation of electric potential  $\delta\phi$  as  $-e\delta n = C\delta\phi$  where  $C = \varepsilon\varepsilon_0/d$  is the gate-channel capacitance per unit area,  $d$  is the gate-channel separation, and  $\varepsilon$  is the dielectric constant of the barrier layer between the gate and the channel. In this case, general solution of the linearized equations for the Fourier harmonics ( $\delta n, \delta v \propto e^{-iqx+i\omega t}$ ) is given by [10]

$$I_\omega = I_1 e^{-iq_1 x} + I_2 e^{-iq_2 x} \quad (2)$$

$$V_\omega = \frac{1}{cW} \left( \frac{I_1}{v_0 + v_p} e^{-iq_1 x} + \frac{I_2}{v_0 - v_p} e^{-iq_2 x} \right),$$

where  $I_1$  and  $I_2$  are the constants to be found from the boundary conditions. Here  $I_\omega = -eW(v_0\delta n + n_0\delta v)$  is the total current and  $V_\omega \equiv \delta\phi_\omega$  is the voltage distribution in the plasma wave of frequency  $\omega$  propagating in the channel of width  $W$ ,  $q_{1,2} = \omega/(v_0 \pm v_p)$  are the wave vectors of the plasma waves propagating in two opposite directions in the channel, and  $v_p = \sqrt{\frac{e^2 n_0}{cm^*}}$  is the plasma velocity in the 2D electron channel at  $v_0 = 0$ .

In the hydrodynamic approximation, the propagation of the plasma waves in the gated 2D electron channel without a dc bias is similar to the propagation of the electromagnetic signals in the transmission line (TL). The linearized hydrodynamic equations for the plasma waves are equivalent to the telegrapher's equations for the TL with the distributed inductance  $\mathcal{L} = \frac{m^*}{e^2 n_0 W}$ , distributed resistance  $\mathcal{R} = \mathcal{L}/\tau$ , and distributed capacitance  $CW$  [17-22]. Consequently, the 2D electron channel can be viewed as a plasmonic waveguide supporting plasma modes [20].

As discussed in Ref. [16], within the TL approach the narrow region of an increased width in Fig. 1 represents an open circuit stub because of the zero-current conditions at the open end with the input impedance

$$Z_{st} = -i \frac{1}{cW_1 v_{p1}} \cot \frac{\omega l}{v_{p1}} \quad (3)$$

Here  $l$  and  $W_1$  are the length and the width of the stub, and  $v_{p1}$  is the plasma velocity in the 2D electron gas in the stub. The value of  $v_{p1}$  is determined by the electron density  $n_{st}$  in the stub and can be controlled independently of  $n_0$  by the separate stub gate. This stub model is valid if the width of the stub  $W_1$  is much smaller than the plasmon wavelength in the channel. Zeros of  $Z_{st}$  correspond to the excitations of the standing plasma modes in the stub with frequencies  $\omega_j = \frac{v_{p1}}{2l} (2j + 1), j = 0, 1, \dots$  [22]. The equivalent TL electric circuit representing field effect transistor (FET) with a stub is shown in Fig. 1b, where the terminating impedances  $Z_{gs}$  and  $Z_{gd}$  describe an electric link between the gate and the source and drain contacts, respectively.

In the presence of constant electron drift, the simple analogy between the hydrodynamic and TL approaches fails because the drifting plasmons carry not only the electromagnetic power adequately described by the simple TL model, but also the kinetic power due to the drift of the electrons oscillating in the plasma wave [10]. The latter effect can be accounted for by introducing the kinetic voltage  $V_{\omega}^{kin} = -m^*v_0\delta v/e$  originally used for description of the space charge waves in electron beams in microwave tubes [23]. Then the total effective voltage  $V_{\omega}^{eff} = V_{\omega} + V_{\omega}^{kin}$  found from Eq. (2) is [10]:

$$V_{\omega}^{eff} = V_{\omega} + V_{\omega}^{kin} = (1 - M^2)V_{\omega} + Z_0MI_{\omega} \quad (4)$$

Here  $M = \frac{v_0}{v_p}$  is the Mach number. The effective voltage  $V_{\omega}^{eff}$  replaces the electric voltage  $V_{\omega}$  in the TL theory of the drifting plasmons. It follows from Eqs. (2) and (4) that the values of  $V_{\omega}^{eff}$  and  $I_{\omega}$  at the opposite boundaries of the dc biased gated 2D electron channel of length  $L$  are connected by the transfer matrix  $\hat{t}$  [10]

$$\hat{t} = e^{-iM\theta} \begin{pmatrix} \cos \theta & iZ_0 \sin \theta \\ \frac{i}{Z_0} \sin \theta & \cos \theta \end{pmatrix}, \quad \theta = \frac{\omega L}{v_p(1-M^2)} \quad (5)$$

where  $Z_0 = \sqrt{\frac{\mathcal{L}}{cW}} = \frac{1}{cWv_p}$  is characteristic impedance of the plasmonic TL representing the FET 2D electron channel. The transfer matrix  $\hat{s}$  relating the values of  $V_{\omega}^{eff}$  and  $I_{\omega}$  across the plasmonic stub in Fig. 1 can be found from the continuity of voltage  $V_{\omega}$  and current conservation in the stub junction

$$\hat{s} = \begin{pmatrix} 1 + \frac{Z_0}{Z_{st}} \frac{M}{1-M^2} & -\frac{Z_0^2}{Z_{st}} \frac{M^2}{1-M^2} \\ \frac{1}{Z_{st}} \frac{1}{1-M^2} & 1 - \frac{Z_0}{Z_{st}} \frac{M}{1-M^2} \end{pmatrix} \quad (6)$$

In these notations, the effective plasmonic voltages and currents near the source ( $V_{\omega,s}^{eff}, I_{\omega,s}$ ) and the drain ( $V_{\omega,d}^{eff}, I_{\omega,d}$ ) boundaries of the conducting channel in the FET structure shown in Fig. 1 are connected as

$$\begin{pmatrix} V_{\omega,s}^{eff} \\ I_{\omega,s} \end{pmatrix} = \hat{t}_1 \hat{s} \hat{t}_2 \begin{pmatrix} V_{\omega,d}^{eff} \\ I_{\omega,d} \end{pmatrix}, \quad (7)$$

where  $\hat{t}_{1,2}$  are the transfer matrices in Eq. (5) for the parts of the 2D channel between the source and the stub, and the stub and the drain with lengths  $L_1$  and  $L_2$ , respectively.

Finding the plasmon dispersion law in the plasmonic cavity formed between the source and the drain requires adding the boundary conditions for Eq. (7). These boundary conditions involving impedances  $Z_{gs}$  and  $Z_{gd}$  are

$$V_{\omega,s} = -Z_{gs}I_{\omega,s} \quad (8)$$

$$V_{\omega,d} = Z_{gd}I_{\omega,d}$$

Solving Eqs. (7) and (8), after some tedious but straightforward algebra we obtain the plasmon dispersion equation

$$e^{i\frac{2\omega L_2}{v_p(1-M^2)}} = \frac{\left(1 + M - \frac{Z_0}{Z_{gd}}\right)\left(1 - M - \frac{Z_0}{Z_{st}} - \frac{Z_0}{Z}\right)}{\left(1 - M + \frac{Z_0}{Z_{gd}}\right)\left(1 + M + \frac{Z_0}{Z_{st}} + \frac{Z_0}{Z}\right)} \quad (9)$$

$$Z = \frac{Z_{gs}(\cos \theta_1 + iM \sin \theta_1) + iZ_0 \sin \theta_1}{[(1 - M^2)Z_{gs} - MZ_0]i \sin \theta_1 + Z_0 \cos \theta_1} Z_0, \quad \theta_1 = \frac{\omega L_1}{v_p(1 - M^2)}$$

The dispersion equation (9) describes the plasma modes in the dc biased FET plasmonic cavity with a stub.

### III. RESULTS AND DISCUSSION

In this section, we use the dispersion equation (9) to demonstrate effect of the stub on the DS instability in the FET structures of different geometry.

In Fig. 2a we show solutions of the dispersion equation (9) for the complex frequencies  $\omega = \omega' + i\omega''$  of the plasma modes in the FET cavity with the stub. For comparison, Fig. 2b shows the solutions for the same cavity but without the stub. In this calculation, we assumed the ideal boundary conditions  $Z_{gs} = 0, Z_{gd} = \infty$ . As expected, the solutions for plasma modes in Fig. 2b reproduce the well-known results first obtained in Ref. [7]. The frequencies  $\omega'$  of the first three plasma modes plotted in units of  $\omega_0 = v_p/L$  take quantized values  $(2n - 1)\pi/2$ ,  $n = 1,2,3$  at zero drift velocity,  $M = 0$ , and gradually decrease when  $M \rightarrow 1$ . The imaginary parts  $\omega''$  are the same for all modes and have negative sign corresponding to the increasing amplitude of the plasma oscillations and instability. At  $M \ll 1$ , we have  $\omega'' = M\omega_0 = v_0/L$  as predicted in Ref. [7]. In Fig. 2a the dispersion equation (9) is solved for the same cavity but with a stub of length  $l = \frac{L}{2}$  positioned in the middle of the cavity,  $L_1 = L_2 = L/2$ , see Fig. 1. For simplicity, we assumed that the widths of the stub and the channel are the same,  $W_1 = W$ , and the 2D electron density in the stub  $n_{st}$  is equal to that in the channel,  $n_{st} = n_0$ . As seen from comparison of Figs. 2a and 2b the stub decreases the plasma frequencies, i.e. decreases the plasma velocities. As pointed out in [16], this makes it easier to implement the plasmonic boom conditions that require the electron drift velocity to rise above the plasma velocity [9, 10]. The effect of the stub on the imaginary part of the frequency (that is on the instability increment) is more pronounced. The degeneracy of the instability increment with respect to the plasma mode number is lifted due to interaction of the plasma modes in the channel with the plasma modes in the stub. In general, the increment tends to decrease because imaginary part of the frequency adds a real component into the stub impedance  $Z_{st}$  in Eq. (3), which effectively decreases the increment. The effect of the stub on the increment is more pronounced for higher harmonics, where the increment can even be reduced to zero at some values of the Mach number (as occurs

for the third mode in Fig. 2a). The frequency of some plasma modes can coincide with one of the frequencies of the standing plasma waves in the stub due to accidental degeneracy leading to  $Z_{st} = 0$ . This effect increases the increment back to its unperturbed value (as occurs for the second mode in Fig. 2a). With all these changes, the instability increment remains robust, and the ability to adjust and optimize both the frequency and the instability increment using the stubs makes the device design with the stubs to be much better suited for THz electronics sources based on the plasmonic instabilities.

This last conclusion is illustrated in Fig. 3, where the frequency and the increment of the fundamental plasma mode in Fig. 2a are plotted as a function of the 2D electron density in the stub,  $n_{st}$ , at two different Mach numbers. The value of  $n_{st}$  can be controlled independently of the 2D electron density  $n_0$  in the channel.

As shown in Fig. 3, the frequency of the instability could be tuned in a wide range (albeit with the changing instability increment). The inset in Fig. 3 shows the dimensionless tunability responsivities. This responsivity is defined as a change of the instability frequency per unit change of the stub gate voltage. We made numerical estimate of the responsivity assuming that its dimensionless value is of the order of unity. For the InGaAs based FET structure with the electron density  $n_0 = 3 \times 10^{15} \text{ m}^{-2}$ , the channel length  $L = 300 \text{ nm}$ , and the gate-to-channel distance  $d = 20 \text{ nm}$ , the responsivity is about 4 GHz/mV showing the possibility of designing a tunable THz source.

The most interesting application of the stub FET structures is the design of the plasmonic system that could have periodic and symmetric boundary conditions and operate at both polarities of the applied bias. One of the main obstacles in designing an effective THz source based on the DS instability is the requirement of the strongly asymmetric boundary conditions at the opposite edges of the plasmonic cavity [7]. The stub design allows one to overcome this obstacle and obtain the DS instability in the FET with symmetric (identical) source and drain contacts. To this end, we investigated the response of the FET with the stub positioned at distances  $L_1$  and  $L_2$  from the source and the drain, respectively,  $L_1 \neq L_2$ ,  $L = L_1 + L_2$ , as shown in Fig. 4d. The stub splits the device into two resonant plasmonic cavities with the effective lengths  $L_1$  and  $L_2$ . We assume that the source and the drain contacts are identical and characterized by the purely reactive impedances  $Z_{gs} = Z_{gd} = ifZ_0$  where  $f$  is some real number. Hence, we neglect the dissipative losses (leakage currents) between the source/drain contacts and the gate.

As shown in Ref. [7], at  $|M| < 1$  the DS instability in the plasmonic cavity develops only if the dc electron drift has direction from the low impedance edge of the cavity to the high impedance one. The instability disappears in the symmetric plasmonic cavity with identical edges. As seen in Fig. 4d, in the symmetric FET with the stub, the instability conditions are always achieved in one of the two split cavities regardless of the direction of the dc current. In Figs. 4a through 4c, we plotted the plasma dispersion curves found from Eq. (9) for the system shown in Fig. 4d at  $f = 0.1, 1, 10$ , respectively. In this calculation, we assumed  $L_1 = 0.3L$  and  $L_2 = 0.7L$  so that the resonant plasma frequencies in the split cavities are different. For the sake of simplicity, we also assumed that the width of the stub is the same as that of the channel,  $W_1 = W$ , and both the stub and the channel have the same 2D electron density,  $n_{st} = n_0$ . The length of the stub  $l$  was chosen to be  $l = 0.2L$  so that  $l < L_1, L_2$ . The last condition prevents the resonant coupling of the low-lying stub and cavity plasma modes, which may result in a decreased instability increment as discussed above. In Fig. 4a, the complex frequencies  $\omega = \omega' + i\omega''$  of the first three unstable plasma modes are plotted as a function of the Mach number

at the value of  $f = 0.1$  corresponding to the near short circuit boundary condition at the source and drain contacts. The plasma frequencies are different at the positive and negative Mach numbers because the instability occurs only in one of the two split cavities of different length dependent on the direction of the dc current. In this limit, the instability increments are very small and can even change sign for the higher harmonics due to coupling between the cavity and the stub plasma modes. In Fig. 4c, the same complex frequencies are shown at the value of  $f = 10$  corresponding to the near open circuit limit at the source and the drain contacts. In this case, the magnitudes of the increment are comparable with the ideal values shown in Fig. 2b. Here, at  $M > 0$  the  $L_2$  cavity contributes to the instability, and at  $M < 0$  the instability occurs in the  $L_1$  cavity. In the intermediate case  $f = 1$  shown in Fig. 4b, the instability increment decreases but remains comparable with the ideal values in Fig. 2b. These results suggest that using the FET with a stub provide ample opportunities to reach plasmonic DS instability in a broad range of the boundary conditions at the source and drain contacts.

This property enables the designs schematically shown in Fig. 5 and 6. As seen from Fig. 5, half of the structure is unstable when the current flows from the source to the drain whereas the other half is unstable for the opposite current direction. In other words, the structure is unstable for both polarities. These designs include many repeating stub-split plasmonic cavity sections working together (and therefore increasing the power) and serving at the same time as an emitting antenna. The biasing scheme shown in these figures makes the bias the same for the repeating sections of the structures. The radiation from these identical sections could be combined coherently. The periodic symmetrical structure shown in Fig. 5a could be scaled in two (Fig. 5b) and three dimensions for an increased power generation. These structures could be used to detect, generate, mix, and multiply THz and/or sub-THz radiation or even far-IR radiation for ultra-short structures.

Fig. 6 shows another implementation that does not require DC contacts and could be pumped by the RF signal and emit the tunable THz radiation. Since the RF frequency is much smaller than the THz emission frequency, the RF bias is equivalent to the DC bias. It could be driven by the RF signal with the frequency much lower than the plasmonic frequencies. Therefore, the structure, if provided with appropriate antennas, could be used as an RF to THz converter. Different THz and RF antenna placements are possible with the optimum design being dependent on the stub parameters and locations.

Recent developments and improvements of the FinFET technology open up the possibility of an alternative stub design with stubs implemented as fins (see Fig. 7). Just as for the stub shown in Fig. 1a, design with multiple periodic or aperiodic stubs is possible (see [24]). A detailed analysis of this structure is beyond the scope of this paper. However, the physics and principle of operation are very similar to the system with the stubs analyzed in this paper.

#### IV. CONCLUSIONS

The presence of stubs enables a wide range tunability of the DS instability frequency and increment and makes it possible to optimize the design of the plasmonic sources, mixers, detectors, and frequency multipliers. It also enables the new designs of multiple frequency sources that could be driven wirelessly. The obtained solutions of the dispersion equation for the device with the stubs in the presence of the electron drift could be used for design and characterization of this new generation of active THz plasmonic devices.

## ACKNOWLEDGMENTS

The work at RPI and CUNY was supported by the US Army Research Office (Project Manager Dr. Joe Qiu)

### References

- [1] M. S. Shur and L. F. Eastman, “*Ballistic Transport in Semiconductors at Low Temperature for Low Power High Speed Logic*”, IEEE Trans. Electron Devices **ED-26**, 1677 (1979).
- [2] M. I. Dyakonov and M. S. Shur, “*Plasma wave electronics: novel terahertz devices using two-dimensional electron fluid*”, IEEE Trans. Electron Devices **43**, 1640 (1996).
- [3] W. Knap, F. Teppe, Y. Meziani, N. Dyakonova, J. Lusakowski, F. Boeuf, T. Skotnicki, D. Maude, S. Rumyantsev, and M. S. Shur, “*Plasma wave detection of sub-terahertz and terahertz radiation by silicon field-effect transistors*”, Appl. Phys. Lett. **85**, 675 (2004).
- [4] T. Otsuji, M. Hanabe, and O. Ogawara, “*Terahertz plasma wave resonance of two-dimensional electrons in InGaP/InGaAs/GaAs high-electron-mobility transistors*”, Appl. Phys. Lett. **85**, 2119 (2004).
- [5] A. El Fatimy, S. Boubanga Tombet, F. Teppe, W. Knap, D. Veksler, S. Rumyantsev, M. Shur, N. Pala, R. Gaska, and Q. Fareed, “*Terahertz detection by GaN/AlGaN transistors*”, Electron. Lett. **42**, 1342 (2006).
- [6] M. Shur, A.V. Muraviev, S. L. Rumyantsev, W. Knap, G. Liu and A. A. Balandin, “*Plasmonic and Bolometric Terahertz Graphene Sensors*”, in *Proceedings of 2013 IEEE Sensors Conference, Baltimore, MD, 2013* (IEEE, New York, 2013), p.1688.
- [7] M. Dyakonov and M. S. Shur, “*Shallow Water Analogy for a Ballistic Field Effect Transistor. New mechanism of Plasma Wave Generation by DC Current*”, Phys. Rev. Lett. **71**, 2465 (1993).
- [8] V. Giliberti, A. Di Gaspare, E. Giovine, M. Ortolani, L. Sorba, G. Biasiol, V. V. Popov, D. V. Fateev, and F. Evangelisti, “*Downconversion of terahertz radiation due to intrinsic hydrodynamic nonlinearity of a two-dimensional electron plasma*”, Phys. Rev. B **91**, 165313 (2015).
- [9] V. Yu. Kachorovskii and M. S. Shur, “*Current-induced terahertz oscillations in plasmonic crystal*”, Appl. Phys. Lett. **100**, 232108 (2012).
- [10] G. R. Aizin, J. Mikalopas, and M. Shur, “*Current-driven plasmonic boom instability in three-dimensional gated periodic ballistic nanostructures*”, Phys. Rev. B **93**.195315 (2016).
- [11] A. El Moutaouakil, T. Suemitsu, T. Otsuji, H. Videlier, S.A. Boubanga-Tombet, D. Coquillat, and W. Knap, “*Device loading effect on nonresonant detection of terahertz radiation in dual grating gate plasmon-resonant structure using InGaP/InGaAs/GaAs material systems*”, Phys. Status Solidi C **8**, 346 (2011).
- [12] A. El Moutaouakil, T. Komori, K. Horiike, T. Suemitsu, and T. Otsuji, “*Room Temperature Intense Terahertz Emission from a Dual Grating Gate Plasmon-Resonant Emitter using InAlAs/InGaAs/InP Material Systems*”, IEICE Trans. Electron. **E93.C**, 1286 (2010).
- [13] Y. M. Meziani, H. Handa, W. Knap, T. Otsuji, E. Sano, V. V. Popov, G. M. Tsymbalov, D. Coquillat, and F. Teppe, “*Room temperature terahertz emission from grating coupled two-dimensional plasmons*”, Appl. Phys. Lett. **92**, 201108 (2008).

- [14] A. S. Petrov, D. Svintsov, V. Ryzhii and M. S. Shur, “*Amplified-reflection plasmon instabilities in grating-gate plasmonic crystals*”, Phys. Rev. B **95**, 045405, (2017).
- [15] V. Kachorovskii and M. Shur, “*Plasmonic Multi Gated FET Crystal as THz Source*”, in *Proceedings of 2012 Lester Eastman Conference on High Performance Devices (LEC)*, Brown University, Providence, RI, 2012 (IEEE, New York, 2012), p. 64.
- [16] G. R. Aizin, J. Mikalopas, M. Shur, “*Plasmons in ballistic nanostructures with stubs: transmission line approach*”, IEEE Trans. Electron. Devices, doi: 10.1109/TED.2018.2854869
- [17] P. J. Burke, I. B. Spielman, J. P. Eisenstein, L. N. Pfeiffer, and K. W. West, “*High frequency conductivity of the high-mobility two-dimensional electron gas*”, Appl. Phys. Lett. **76**, 745 (2000).
- [18] I. Khmyrova and Yu. Seijyou, “*Analysis of plasma oscillations in high-electron mobility transistor like structures: distributed circuit approach*”, Appl. Phys. Lett. **91**, 143515 (2007).
- [19] G. C. Dyer, G. R. Aizin, S. Preu, N. Q. Vinh, S. J. Allen, J. L. Reno, and E.A. Shaner, “*Inducing an incipient terahertz finite plasmonic crystal in coupled two-dimensional plasmonic cavities*”, Phys. Rev. Lett. **109**, 126803 (2012).
- [20] G. R. Aizin and G. C. Dyer, “*Transmission line theory of collective plasma excitations in periodic two-dimensional electron systems: Finite plasmonic crystal and Tamm states*”, Phys. Rev. B **86**, 235316 (2012).
- [21] G. C. Dyer, G. R. Aizin, S. J. Allen, A. D. Grine, D. Bethke, J. L. Reno, and E. A. Shaner, “*Induced transparency by coupling of Tamm and defect states in tunable terahertz plasmonic crystals*”, Nat. Photonics **7**, 1925 (2013).
- [22] H. Yoon, K. Y. M. Yeung, P. Kim, D. Ham, “*Plasmonics with two-dimensional conductors*”, Phil. Trans. R. Soc. A **372**: 20130104 (2014).
- [23] W. J. Kleen, *Electronics of microwave tubes*, (Academic Press, New York, 1958).
- [24] W. Stillman, C. Donais, S. Rumyantsev, M. Shur, D. Veksler, C. Hobbs, C. Smith, G. Bersuker, W. Taylor and R. Jammy, “*Silicon FIN FETs as detectors of terahertz and sub-terahertz radiation*”, Int. J. Hi. Spe. Ele. Syst. **20**, 27 (2011).

### Figure captions

Figure 1. Stub configuration (a) and its transmission line (TL) equivalent circuit (b).

Figure 2. Real ( $\omega'$ ) and imaginary ( $\omega''$ ) parts of the plasmonic frequency versus Mach number  $M$  in the FET: (a) with the stub ( $l = L/2$ ,  $W_1 = W$ ,  $n_{st} = n_0$ ); (b) without the stub.  $Z_{gs} = 0$ ,  $Z_{gd} = \infty$ ,  $\omega_0 = v_p/L$

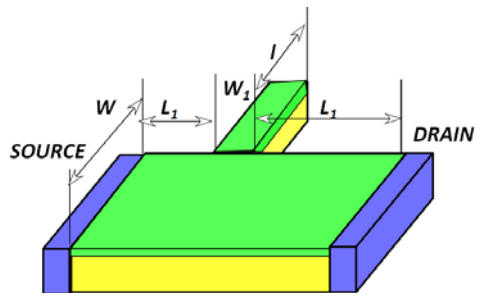
Figure 3. The stub FET fundamental plasmonic frequency  $\omega'$  and the instability increment  $\omega''$  as a function of the 2D electron density in the stub  $n_{st}$  at two different Mach numbers  $M$ ,  $n_0$  is 2D electron density in the FET channel. Other parameters are the same as in Fig. 2a. Inset: the tunability responsivity as a function of  $n_{st}$ .

Figure 4. The plasmonic frequencies  $\omega'$  and the instability increments  $\omega''$  as a function of the Mach number  $M$  in the stub FET with symmetric boundaries:  $Z_{gs} = Z_{gd} = ifZ_0$ . (a)  $f=0.1$ ; (b)  $f=1$ ; (c)  $f=10$ . In this calculation:  $l = 0.2L$ ,  $L_1 = 0.3L$ ,  $L_2 = 0.7L$ , other parameters are the same as in Fig.2a. (d) Schematic diagram and the equivalent TL electric circuit of the stub FET.

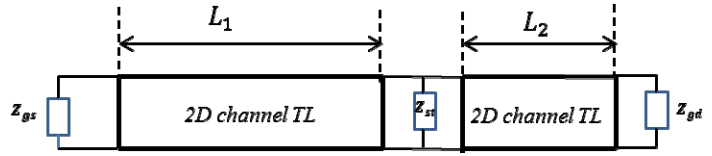
Figure 5. The stub-split plasmonic cavity periodic design: linear (a) and two-dimensional (b) configurations.

Figure 6. The RF driven stub-split cavity RF to THz converter section (a) and periodic arrangement (the plasmonic converter crystal) (b).

Figure 7. Fin-like stub (a) and multiple Fin stubs (b).

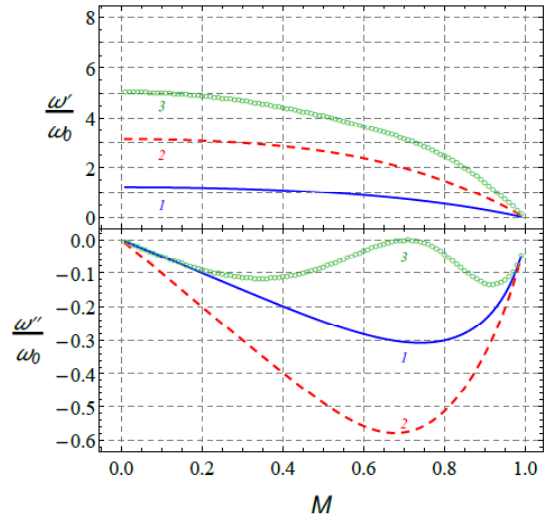


(a)

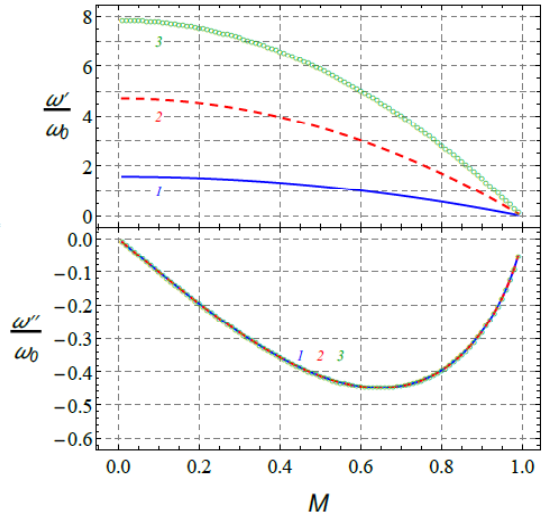


(b)

Figure 1



(a)



(b)

Figure 2

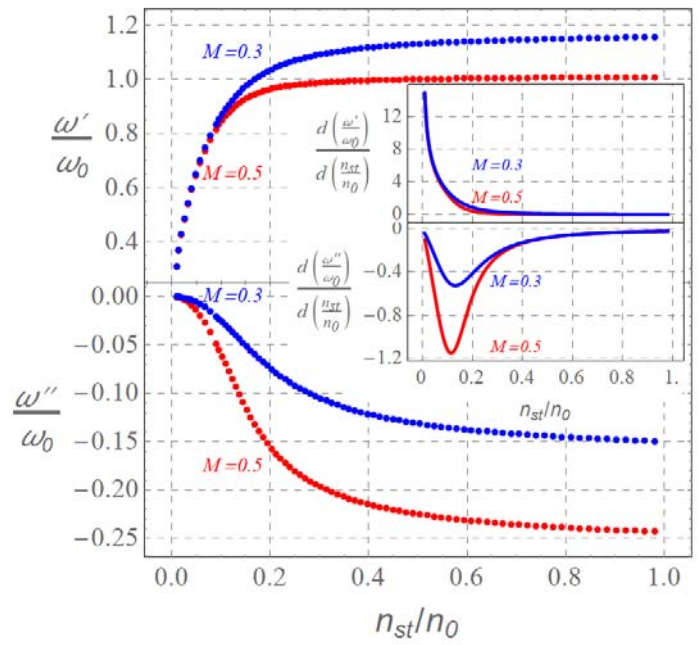
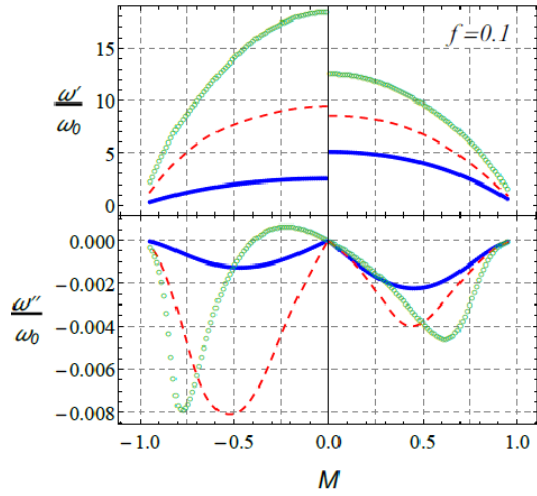
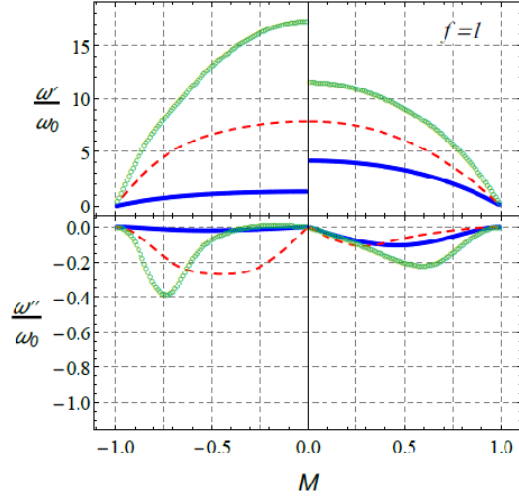


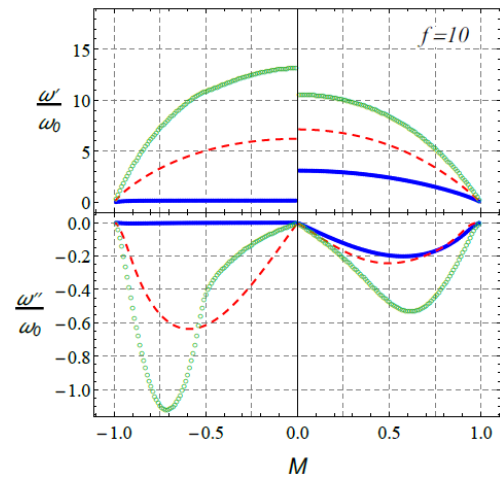
Figure 3



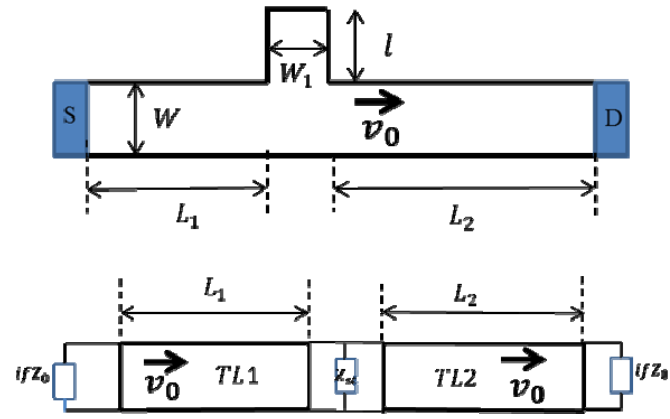
(a)



(b)



(c)



(d)

Figure 4

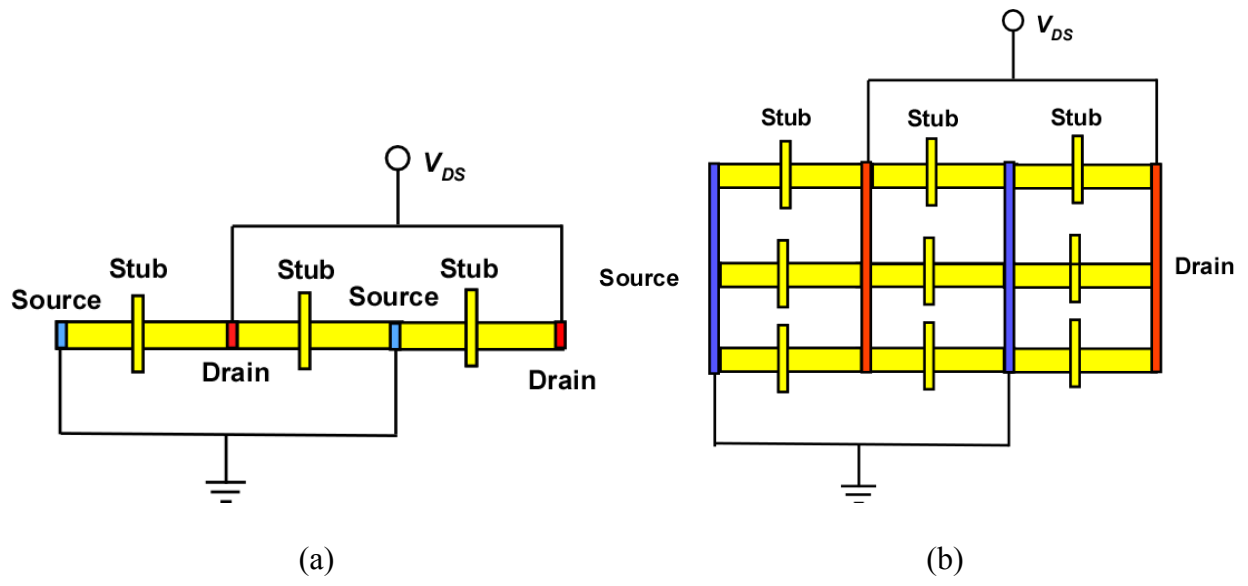


Figure 5

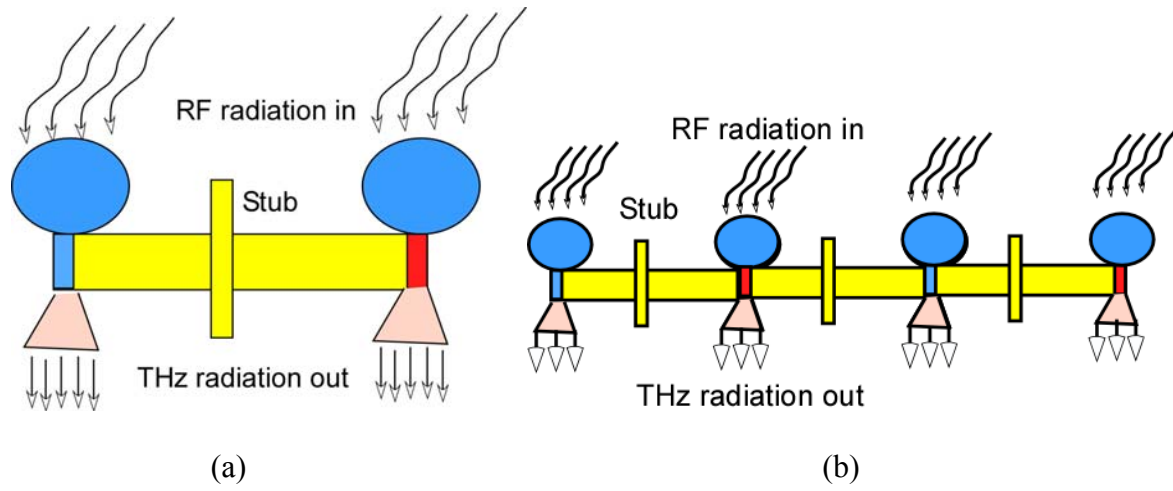
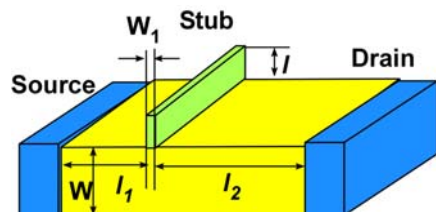
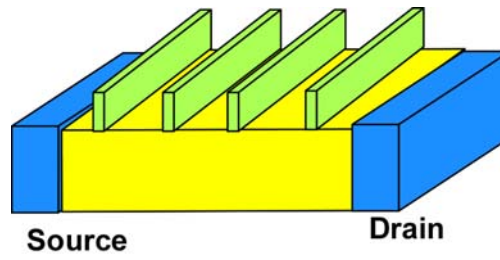


Figure 6



(a)



(b)

Figure 7